Impact of Wiring Characteristics on Voltage-based Fingerprinting in Controller Area Networks

Lucian Popa, Camil Jichici, Tudor Andreica, Pal-Stefan Murvay and Bogdan Groza

Faculty of Automatics and Computers
Politehnica University of Timisoara, Timisoara, Romania
Email: lucian.popa@aut.upt.ro, camil.jichici@aut.upt.ro, tudor.andreica@aut.upt.ro,
pal-stefan.murvay@aut.upt.ro, bogdan.groza@aut.upt.ro

Abstract—Voltage patterns generated by Controller Area Network (CAN) nodes have been commonly proposed as a source for sender identification as this exposes fine grain manufacturing characteristics. However, the influence of wiring on voltage patterns was insufficiently studied so far and it may be critical in understanding the accuracy of the fingerprinting process. Here we study the influence of wiring on three voltage characteristics: slew rate distribution of recessive to dominant transitions, peak-to-peak and peak-to-root mean square distributions on the plateau area of a dominant bit. Using collected voltage data, we identify slew rate variations depending on the wiring used in each experimental setup. Voltage patterns collected in a laboratory setup with automotive grade cables seem to be identical with those from real-world vehicles, which suggests that this type of cables should be used for realistic experiments.

Index Terms—CAN, voltage, fingerprints, wiring

I. INTRODUCTION AND RELATED WORK

Controller Area Network (CAN) is a widely used communication protocol that connects Electronic Control Units (ECUs), sensors or actuators inside vehicles. This is due to its robustness and reliability in severe environmental conditions, such as extreme temperatures or high humidity. However, in the past decade, there have been multiple recorded attacks involving the CAN bus [1], [2]. These threats have prompted the development of protective measures such as vulnerability testing [3], [4]. Another topic of interest for automotive security, that was the main topic in a number of recent studies [5]–[7], are physical fingerprinting techniques, which can be used to identify if a source is legitimate or adversarial. Since these methods take into account minute features of the bus voltage level, evaluating the influence of wiring is important. Clearly, it is unlikely for wiring changes to occur inside a car after it was manufactured, but many research works use experimental setups which are not built using automotive grade wires [5], [8]. Therefore, in this work we try to gain more insights into cabling influence on voltage patterns.

Since the original design of the CAN bus lacks message origin authentication, additional security controls must be implemented to prevent attacks that could cause significant harm. While there are multiple proposals for CAN authentication [9], [10], many of them require modifications to the CAN standard, require extended payloads and lead to increased communication overheads. To overcome these limitations, a series of studies use voltage characteristics to identify and authenticate the source of messages and detect ECUs that transmit malicious frames. A voltage-based Intrusion Detection System (IDS), named VoltageIDS, that leverages the unique characteristics of CAN electrical signals is presented in [6]. The IDS was tested using data from a CAN bus prototype made of Arduino boards and real-world CAN data collected from two vehicles. The authors in [8] propose an identification approach that operates at the physical layer of the CAN bus and requires the addition of a monitoring ECU. The approach works with the CAN extended frame format. In [5], the authors used voltage profiles and acknowledge bit (ACK) voltage thresholds from CAN frames to fingerprint ECUs and detect malicious devices. The approach was evaluated in an experimental setup as well as on CAN networks from a Honda Accord and a Chevrolet Trax. Another fingerprinting method that uses CAN signals, called Scission, is presented in [7]. During tests performed on a prototype and two real vehicles, Scission was able to accurately identify the sender of each message with a 99.85% true positive rate. By recognizing the particular voltage signal characteristics of each ECU, a more recent work [11] demonstrated the ability to detect attacks from external nodes and internal compromised ECUs.

CAN with Flexible Data Rate (CAN-FD) was introduced in order to cope with the demanding communication speed requirements of autonomous vehicles [12]. However, the increased speed may potentially cause even more physical signal quality issues. In what follows, we discuss some works that address such issues. When a CAN-FD bus prototype is designed, propagation delays which can be induced by the transmission medium and signal distortion, i.e., ringing effect, are taken into account [13]. Electromagnetic emissions caused by CAN-FD transmitters can disturb the behavior of other automotive integrated circuits and represent another factor which must be considered in the deployment of such transmitters [14]. On the other hand, there might be instances where additional hardware components, e.g., a buck converter, positioned close to the CAN wires, may cause noise during CAN communication through electromagnetic interference [15]. The authors from [15] propose a method to eliminate the induced noise by temporarily holding the signal based on the converter switching timings in order to mask logical flips in the receiver output. In the light of the above, regardless of the protocol that is used, i.e., CAN or CAN-FD, since the transmission

medium is the same, voltage patterns such as noise or ringing effects will have a negative impact on source fingerprinting and identification.

The main contributions of this work are:

- Collection of a voltage dataset from the CarTwin [16] experimental setup,
- Extraction of three voltage features, i.e., slew rate, peak-to-peak and peak-to-root mean square, from four distinct voltage datasets,
- Analysis and evaluation of the voltage features that emphasize the importance of CAN wirings used in voltage fingerprinting activities.

The remainder of this paper is organized as follows. In Section II we present an overview of the CAN bus and tools followed by a description of the experimental setups as well as the datasets that were used as basis for the analysis we performed. Section III presents the framework for data analysis followed by evaluation of the wiring impact using specific voltage features. Finally, Section IV concludes the results of this work.

II. DETAILS ON EXPERIMENTS

In this section we discuss some brief background and give details on the experimental setups and datasets that we use.

A. Background and Tools

The CAN protocol, developed by BOSCH [17] in the 1980s and then standardized by the International Organization for Standardization (ISO) as ISO 11898 [18], [19], is still the most popular automotive bus due to its simplicity, cost and reliability. A simple two-wire CAN-High (CAN-H) and CAN-Low (CAN-L) differential bus terminated with two 120Ω resistors is used to transmit data which is encoded as logical "0" (dominant state) or logical "1" (recessive state).

Figure 1 depicts the physical and logical high-speed CAN bit representation. When the bus is idle, or a recessive bit is broadcast, the voltage for both CAN-H and CAN-L is roughly 2.5V. In contrast, the dominant state occurs when the CAN-L drops close to 1.5V and the voltage on CAN-H is around 3.5V. Data transmissions are formatted as CAN data frames (Figure 2). Each frame starts with a dominant bit, called SOF (Start-of-frame), followed by the arbitration field, which contains the CAN identifier (ID) (11 bits for standard frames or 29 bits for extended frames). Besides uniquely identifying a message, the CAN ID is also used for arbitration, i.e, high priority is assigned to lower valued IDs. The subsequent field is the control field that contains the data length code (DLC) which indicates the number of bytes (maximum 8 for CAN standard) that are packed into the data field. A 15-bit cyclic redundancy check (CRC) and the acknowledge (ACK) bit, which is used to confirm that network nodes have been properly received a frame, follow after the data field. Finally, a set of recessive EOF (End-of-frame) bits mark the end of each frame.

Before detailing the experimental setups and datasets we also give some hints on the the tools we used to collect voltage samples and the tool configurations. We collected voltage data
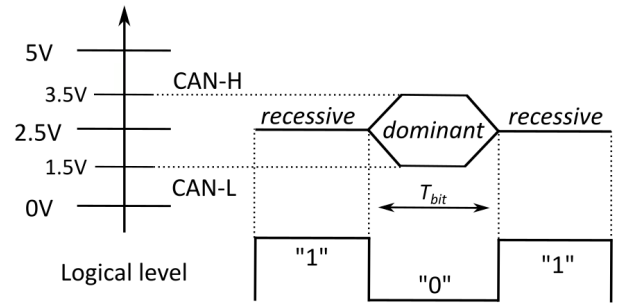
Fig. 1. High speed CAN bit representation at the physical and logical level
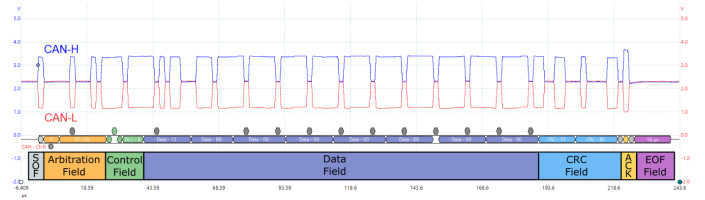
Fig. 2. CAN-H and CAN-L voltage samples for a CAN frame with details on bit fields

using a 5000 series PicoScope. The same device was used to collect voltage data in several other works [20]–[22] on which we rely in this paper.

The PicoScope supports sampling based on configured triggers so we used this to sample CAN voltage data based on the rising edge of the CAN-H line that corresponds to the transition on the bus between the recessive state to the dominant state. Voltage data for an entire CAN frame is shown in Figure 2 with details for its structure, i.e., SOF, arbitration, control, data, CRC, ACK and EOF fields.

For statistical analysis on the voltage data collected for this work or from existing datasets we used MATLAB R2022a. Details related to statistical features extracted from the datasets will be provided in the upcoming section.

B. Brief description of the employed experimental setups

Next, we describe the experimental setups and provide details on the cables used (including AWG, i.e., American wire gauge) in each case to obtain the datasets that we analyze in this paper.

TIDAL-CAN. The experimental setup from *TIDAL-CAN* [20] employed 10 CAN nodes, each node being connected at a specific distance from the others. The cable is built as a set of twisted wires (a pair of CAN lines and a ground wire) with a length of $5m$ and a termination of 120Ω on both ends. The wires are basic wires with a solid bare copper conductor of $0.6mm^2$ (19 AWG) and an individual cable diameter of $3.1mm$, including insulation.

CAN-SQUARE. The experimental setup from *CAN-SQUARE* [21] has 5 CAN nodes connected on the CAN bus on the clean setup and up to 8 nodes when 3 adversarial nodes are present. Here, a $5m$ industry grade CAN bus cable was used to connect the nodes. The terminations used on both sides

Experimental Setup	Wire type and its cross-section (AWG)	Wiring	Grade
TIDAL-CAN [20]	Solid Bare Copper Wire of $0.6mm^2$ (19 AWG)	Unshielded Twisted pair (UTP)	Off-the-shelf
CAN-SQUARE [21]	Stranded Copper Wire of $0.22mm^2$ (24 AWG)	Shielded Twisted Pair (STP)	Industrial
CarTwin [16]	Stranded Copper Wire of $0.5mm^2$ (20 AWG)	Unshielded Twisted Pair (UTP)	Automotive
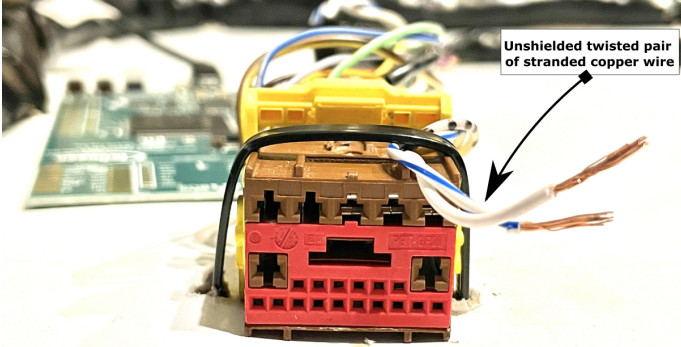
Fig. 3. Wires from the automotive wiring harness that is part of *CarTwin* [16] experimental setup

of the network were split terminations consisting of $2 \times 60\Omega$ resistors connected in series together with a $10nF$ capacitor with the intent to reduce noise. The wires from the CAN bus cable are shielded with a copper-tinned braid and have a $0.22mm^2$ (24 AWG) copper conductor with an individual wire diameter of $0.6mm$, including insulation, and a total cable harness diameter of $5.4mm$.

CarTwin. There are 8 nodes connected on the CAN bus from the experimental setup designed in *CarTwin* [16]. The CAN bus consists of three interconnected wiring harnesses from a real-world vehicle where the CAN wires were pre-served along the entire harness length. Excluding the stubs and splices, the main wire length is of $\sim 5.1m$ while the stubs vary in length from $0.5m$ to $1.2m$, depending on the original position in the vehicle. The 120Ω termination on both sides of the CAN bus was preserved on two AURIX TC275 Lite kits since they already had it on the PCB and it was removed from the other nodes in order to achieve the required bus impedance. According to the *Wiring Diagram Handbook* of the vehicle from which we used the harnesses, the CAN bus wires have a $0.5mm^2$ (20 AWG) copper conductor with an individual cable diameter of $2.5mm$.

A summary of wire types, wire cross-section, equivalent AWG, wiring and grade considered for the wires, e.g., indus-trial, is presented in Table I. The wires from an automotive grade wiring harness used in the *CarTwin* [16] experimental setup is shown in Figure 3.

C. Datasets from existing works

In what follows, we provide details for the collected voltage datasets from the experimental setups used in *TIDAL-CAN* [20], *CAN-SQUARE* [21] and *CarTwin* [16]. In our analysis we also include the *ECUPrint* [22] dataset that was collected

from real-world vehicles in order to provide a comparative example to the experimental setup voltage data.

The dataset from the *TIDAL-CAN* [20] experimental setup contains voltage data for the CAN-H line from 1000 individual CAN frames for each experiment that is collected with the PicoScope configured for a window size of $2\mu s$ and a sample step of $1ns$. For collecting the dataset from the *CAN-SQUARE* [21] experimental setup, the PicoScope was configured with the same window size as for *TIDAL-CAN* [20] but with a sample step of $2ns$ or $4ns$ since in this work there is voltage data collected from both CAN-H and CAN-L lines from 500 individual CAN frames for each experiment. For the *ECUPrint* [22] dataset, the window size was configured to $2ms$ with a sample step of $2ns$ in order to capture multiple CAN frames in the same window with a low sample step, as in the previous works. As Table 1 from the *ECUPrint* [22] paper shows, voltage samples of multiple bits are collected in the dataset, e.g., $\sim$32k individual bits for Dacia Logan, etc.

The dataset collected from the *CarTwin* [16] experimental setup is done as a contribution for the current work. Thus, we have collected a number of 250 voltage sample windows of $2ms$ from the setup, in the same way we did for collecting voltage data from the vehicles in *ECUPrint* [22]. This results in voltage samples collected for a total number of 916 individual frames from the *CarTwin* [16] experimental setup which are used in the evaluation part of this work.

III. EXPERIMENTAL EVALUATION OF WIRING IMPACT

In this section we present the data analysis framework used to evaluate voltage characteristics extracted from signals in the datasets. Then, we illustrate the histogram distributions for three voltage characteristics from the experimental setup datasets and one real-world vehicle dataset: recessive to dom-inant transition slew rate, peak-to-peak on the plateau area of a dominant bit and peak-to-root mean square for the same bit area.

A. Framework for data analysis

Dataset alignment. In order to analyze the voltage profiles on different cables from the experimental setups in a com-parative manner, we separate the rising edges for the CAN-H voltage line from all datasets. This is required since in the samples collected for *TIDAL-CAN* [20] and *CAN-SQUARE* [21] only the edges for transitions between recessive and dominant bits (and also a part of the dominant bit plateau) are present. We use a total of 500 voltage samples over $2\mu s$, i.e., bit time for a data rate of 500Kbps, which corresponds to a sample rate of $4ns$. We do this in order to align the measurements to the lowest sample rate from our datasets.
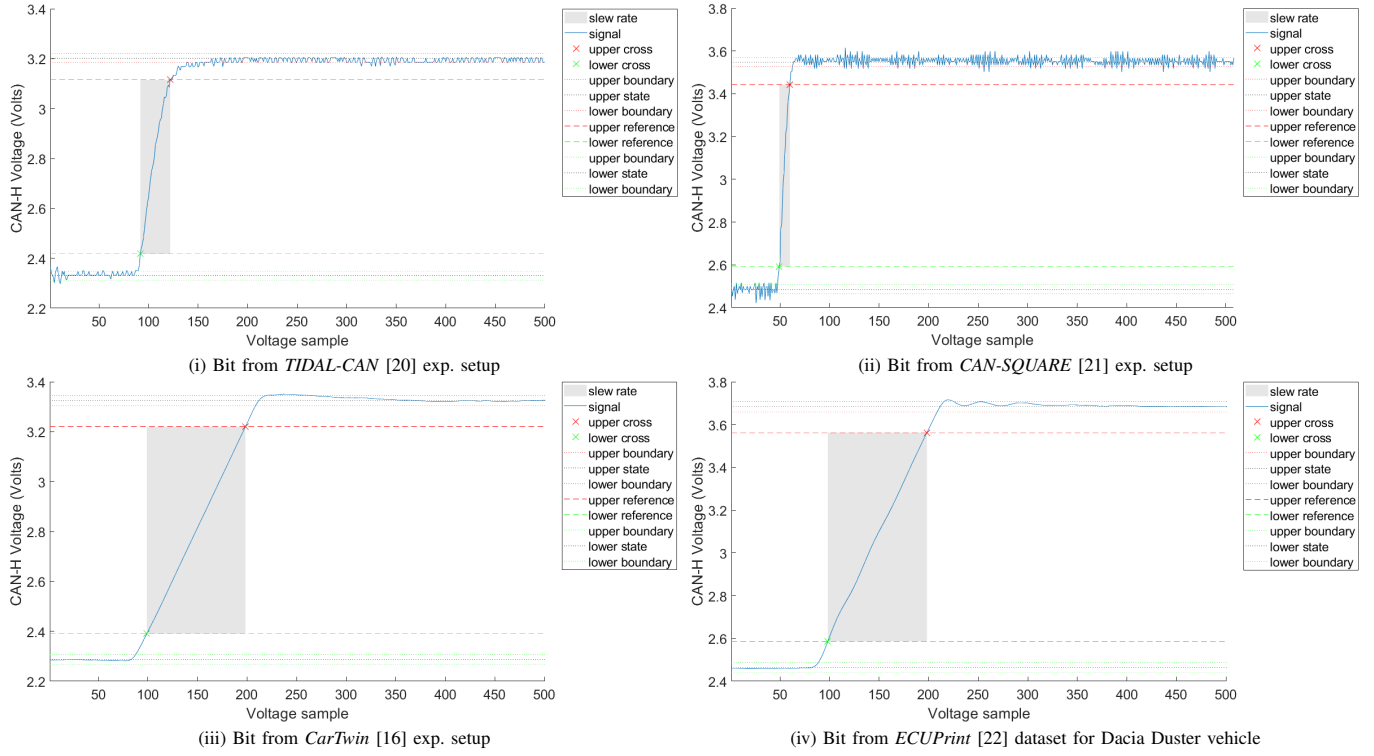
Fig. 4. The slew rate represented in MATLAB for the CAN-H rising edge of a bit collected in the *TIDAL-CAN* [20] experimental setup (i), *CAN-SQUARE* [21] experimental setup (ii), *CarTwin* [16] experimental setup (iii) and the *ECUPrint* [22] dataset (iv)
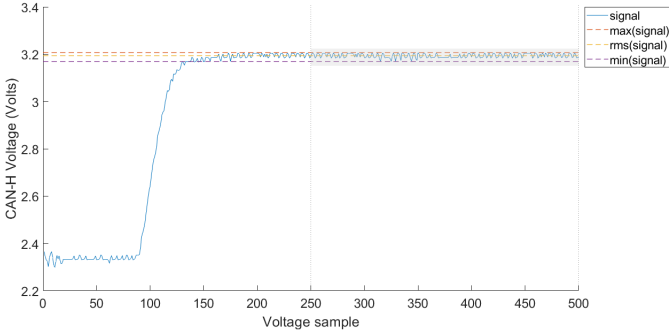
Fig. 5. The V_{P2P} (V_{min} to V_{max}) and V_{RMS} values represented in MATLAB for the CAN-H dominant plateau area of a bit collected in the *TIDAL-CAN* [20] exp. setup

Slew rate. The slew rate for a voltage signal represents the absolute value of voltage change over time. It can be measured over a specified voltage range of the rising or falling period. Hence, we measured the slew rate for the transition between recessive and dominant CAN bits (SR_{CAN}) as absolute value of difference between 90% and 10% of the CAN-H voltage rise time over the time difference, as described in Equation 1. This is visually depicted in Figure 4, in the gray area delimited by the red and green dashed lines, for bits collected from all experimental setups (i), (ii), (iii) or the vehicle (iv).

$$SR_{CAN} = (|\frac{V_{90\%} - V_{10\%}}{\Delta t}|) \quad (1)$$

Peak-to-peak and peak to root mean square value. In order to determine the statistical features from the datasets we use the peak-to-peak (x_{P2P}), root mean square (x_{RMS}) and the peak to root mean square (x_{P2RMS}) values of the voltage signal. The peak-to-peak (x_{P2P}) value for a signal x shown in Equation 2 is represented by the difference between maximum and minimum values for a given sample range. The root mean square (x_{RMS}) value for a signal x over N samples shown in Equation 3 is computed as square root of the mean value of the sample square sum. The peak to root mean square (x_{P2RMS}) value shown in Equation 4 is computed as ratio between the maximum value for a given signal range and its root mean square value. An example of the V_{min}, V_{max} and V_{RMS} values computed on 250 voltage samples from the plateau area of a bit is shown in the gray area of Figure 5.

$$x_{P2P} = max(x) - min(x) \quad (2)$$

$$x_{RMS} = (\sqrt{\frac{1}{N} \sum_{n=1}^{N} x_n^2}) \quad (3)$$

$$x_{P2RMS} = \frac{max(x)}{x_{RMS}} \quad (4)$$

B. Experimental results and discussions

As experiments conducted in this work we present the computed slew rate distribution for 1500 bits transmitted by the VN5610A device from Vector, 500 bits from each

(i) SR_{CAN} for VN1650A in *TIDAL-CAN* [20] exp. setup

(ii) SR_{CAN} for VN1650A in *CAN-SQUARE* [21] exp. setup

(iii) SR_{CAN} for VN1650A in *CarTwin* [16] exp. setup

(iv) SR_{CAN} for ECU1 in the Dacia Duster from *ECUPrint* [22] dataset
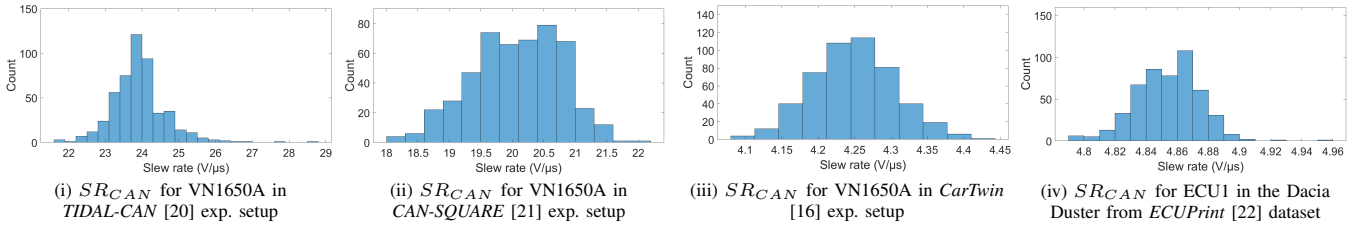
Fig. 6. The SR_{CAN} (slew rate) distribution for 500 bits transmitted by Vector VN5610A in the *TIDAL-CAN* [20] experimental setup (i), *CAN-SQUARE* [21] experimental setup (ii), *CarTwin* [16] experimental setup (iii) and by ECU1 in the Dacia Duster from the *ECUPrint* [22] dataset (iv)

(i) V_{P2P} for VN1650A in *TIDAL-CAN* [20] exp. setup

(ii) V_{P2P} for VN1650A in *CAN-SQUARE* [21] exp. setup

(iii) V_{P2P} for VN1650A in *CarTwin* [16] exp. setup

(iv) V_{P2P} for ECU1 in the Dacia Duster from *ECUPrint* [22] dataset
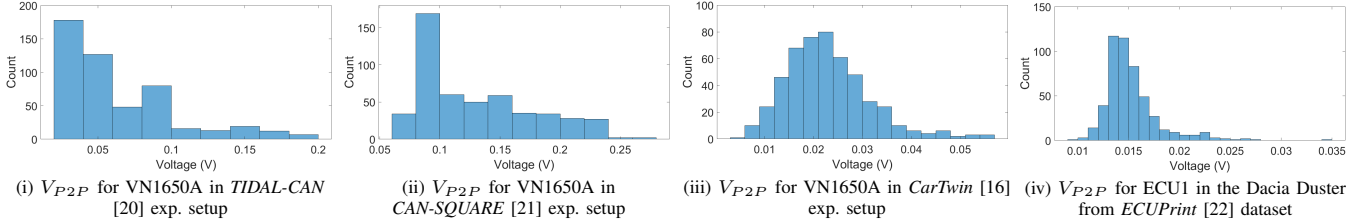
Fig. 7. The V_{P2P} (voltage peak-to-peak) distribution for 500 bits transmitted by Vector VN5610A in the *TIDAL-CAN* [20] experimental setup (i), *CAN-SQUARE* [21] experimental setup (ii), *CarTwin* [16] experimental setup (iii) and by ECU1 in the Dacia Duster from the *ECUPrint* [22] dataset (iv)

(i) V_{P2RMS} for VN1650A in *TIDAL-CAN* [20] exp. setup

(ii) V_{P2RMS} for VN1650A in *CAN-SQUARE* [21] exp. setup

(iii) V_{P2RMS} for VN1650A in *CarTwin* [16] exp. setup

(iv) V_{P2RMS} for ECU1 in the Dacia Duster from *ECUPrint* [22] dataset
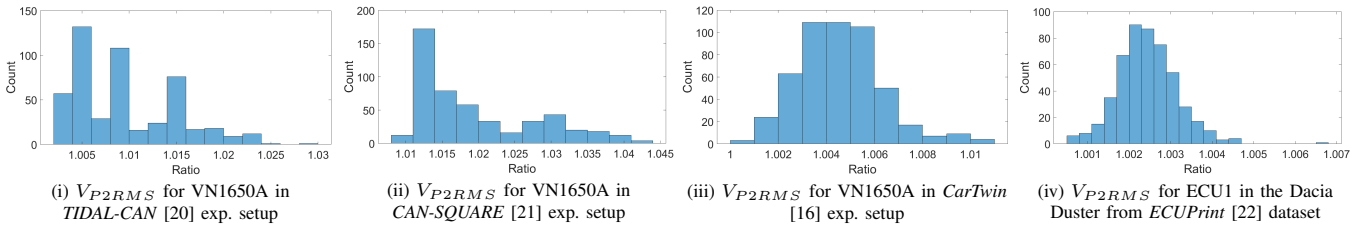
Fig. 8. The V_{P2RMS} (voltage peak-to-RMS) distribution for 500 bits transmitted by Vector VN5610A in the *TIDAL-CAN* [20] experimental setup (i), *CAN-SQUARE* [21] experimental setup (ii), *CarTwin* [16] experimental setup (iii) and by ECU1 in the Dacia Duster from the *ECUPrint* [22] dataset (iv)

experimental setup previously described and additionally 500 bits from the *ECUPrint* [22] dataset as comparative values from a car. Then, we detail the noise analysis conducted on the same bits using the $P2P$, and $P2RMS$ distributions.

Slew rate distribution. The slew rate value (SR_{CAN}) is computed in MATLAB as the ratio between voltage difference (90% to 10% during rise time) and time difference for the values, as already shown in Figure 4. The slew rate distribution from *TIDAL-CAN* [20] for the Vector device contains values in the 21–29 $V/\mu s$ range with most of the values in the 23–25 $V/\mu s$ range as shown in Figure 6 (i). In the *CAN-SQUARE* [21] data, the slew rate distribution has bins with lower values for the same device. Figure 6 (ii) presents values in the 18–22 $V/\mu s$ range while most of the values are in the 19–21 $V/\mu s$ range. Finally, the slew rate distribution for the VN5610A used in the *CarTwin* [16] setup from Figure 6 (iii) is much lower, in the 4.10–4.45 $V/\mu s$ range while most of the values reside in the 4.2–4.3 $V/\mu s$ range. As comparative voltage values in the dataset collected from the vehicles for *ECUPrint* [22], the slew rate for ECU1 from Dacia Duster varies between 4.7 $V/\mu s$ and 5 $V/\mu s$, as shown in the Figure 6 (iv). By comparing the distributions for the same device, i.e., Vector VN5610A, it is apparent that usage of a commercial, industrial or automotive grade cable as transmission medium has an influence on the transition time between the recessive

and dominant states. Furthermore, the slew rate distribution for the *CarTwin* [16] setup is the closest to the one from the real-world vehicle (slew rate of below 10 $V/\mu s$). This is expected since the cable used in the experimental setup from *CarTwin* [16] comes from a real-world vehicle.

Peak-to-peak distribution. To measure the signal variation over time we look at the peak-to-peak voltage (V_{P2P}) over 250 samples from each bit for a total of 500 bits while the CAN bus is already in the dominant state, as already shown in the gray area from Figure 5. The V_{P2P} values for VN5610A communicating in the *TIDAL-CAN* [20] experimental setup vary from $25mV$ to $200mV$ with most of the values below $100mV$, as shown in Figure 7 (i). The V_{P2P} distribution for the same device in the *CAN-SQUARE* [21] experimental setup shown in Figure 7 (ii) contains values in the $50mV$–$275mV$ range while most values are below $150mV$. The variation between the maximum and minimum value, i.e., peak to peak, decreases for the *CarTwin* [16] experimental setup data to a range of $5mV$ to $55mV$ as presented in Figure 7 (iii). The peak-to-peak distribution for ECU1 in the Dacia Duster vehicle from *ECUPrint* [22] shown in Figure 7 (iv) has values in the $9mV$–$35mV$ range with most of the values below $20mV$. There are higher V_{P2P} values in the *TIDAL-CAN* [20] and *CAN-SQUARE* [21] measurements compared to those from the *CarTwin* [16] and *ECUPrint* [22] which strengthens our

beliefs that the cable used has an influence on the CAN voltage patterns. We also consider that lowering the wire cross-section will increase the noise over the original signal voltage, i.e., higher V_{P2P} values for *CAN-SQUARE* [21] (wire cross-section of $0.22mm^2$) compared to values for *TIDAL-CAN* [20] (wire cross-section of $0.6mm^2$).

Peak-to-RMS distribution. Now we detail the voltage peak to root mean square (V_{P2RMS}) distribution for each experimental setup that was computed in the same way as the V_{P2P} distribution. The ratio between the maximum voltage value (V_{max}) and the voltage RMS (V_{RMS}) value for the *TIDAL-CAN* [20] data, shown in Figure 8 (i), is in the range of 1.004 to 1.030 which means that the maximum value is with up to 3% higher than the RMS value. For the *CAN-SQUARE* [21] distribution depicted in Figure 8 (ii) the ratio is a bit higher, with values between 1.010 and 1.040 so the maximum value is at least 1% higher and with up to 4% higher than the V_{RMS}. Comparative results are shown in Figures 8 (iii) and (iv) because the range for the ratio distribution for *CarTwin* [16] data is of 1.000 to 1.011 while the ratio distribution for the Dacia Duster ECU data from *ECUPrint* [22] is of 1.001 to 1.007. Thus, in this case, the maximum value is up to 1% higher than the voltage RMS (V_{RMS}) value. We consider the differences between V_{P2RMS} distributions are caused by the cables in the same way cables affect the V_{P2P} distributions.

IV. CONCLUSION

By analyzing the voltage dataset collected, for this work, with the help of the CarTwin experimental setup in contrast with existing datasets from TIDAL-CAN [20], CAN-SQUARE [21] we observed that a higher slew rate and noise are present in networks where commercial or industrial grade cables are used. Clearly, the induced noise is influenced by the types of wiring that are used and in order to have an experimental setup as close as possible to the real vehicle conditions an automotive grade harness is highly recommended. Fortunately, in case of both TIDAL-CAN [20], CAN-SQUARE [21], the localization procedure should not be heavily affected by the noise of the electric signal. But more demanding works for ECU classification based on voltage levels may be more affected.

ACKNOWLEDGMENT

REFERENCES

[1] S. Checkoway, D. McCoy, B. Kantor, D. Anderson, H. Shacham, S. Savage, K. Koscher, A. Czeskis, F. Roesner, T. Kohno *et al.*, "Comprehensive experimental analyses of automotive attack surfaces." in *USENIX security symposium*. San Francisco, 2011, pp. 1–16.

[2] C. Miller and C. Valasek, "A survey of remote automotive attack surfaces," *black hat USA*, p. 90, 2014.

[3] S. Hariharan, A. V. Papadopoulos, and T. Nolte, "On in-vehicle network security testing methodologies in construction machinery," in *27th International Conference on Factory Automation (ETFA)*, 2022, pp. 1–4.

[4] T. Brennich and M. Moser, "Putting automotive security to the test," *ATZelectronics worldwide*, vol. 15, no. 1, pp. 46–51, 2020.

[5] K.-T. Cho and K. G. Shin, "Viden: Attacker identification on in-vehicle networks," in *Proceedings of the 2017 ACM SIGSAC Conference on Computer and Communications Security*, 2017, pp. 1109–1123.

[6] W. Choi, K. Joo, H. J. Jo, M. C. Park, and D. H. Lee, "VoltageIDS: Low-level communication characteristics for automotive intrusion detection system," *IEEE Transactions on Information Forensics and Security*, vol. 13, no. 8, pp. 2114–2129, 2018.

[7] M. Kneib and C. Huth, "Scission: Signal characteristic-based sender identification and intrusion detection in automotive networks," in *Proceedings of the 2018 ACM SIGSAC Conference on Computer and Communications Security*, 2018, pp. 787–800.

[8] W. Choi, H. J. Jo, S. Woo, J. Y. Chun, J. Park, and D. H. Lee, "Identifying ECUs using inimitable characteristics of signals in controller area networks," *IEEE Transactions on Vehicular Technology*, vol. 67, no. 6, pp. 4757–4770, 2018.

[9] B. Groza, P.-S. Murvay, A. Van Herrewege, and I. Verbauwhede, "LiBrA-CAN: a lightweight broadcast authentication protocol for controller area networks," in *11th International Conference on Cryptology and Network Security, CANS 2012, Springer-Verlag, LNCS*, 2012.

[10] G. Bella, P. Biondi, G. Costantino, and I. Matteucci, "Toucan: A protocol to secure controller area network," in *Proceedings of the ACM Workshop on Automotive Cybersecurity*, 2019, pp. 3–8.

[11] Y. Xun, Z. Deng, J. Liu, and Y. Zhao, "Side channel analysis: A novel intrusion detection system based on vehicle voltage signals," *IEEE Transactions on Vehicular Technology*, pp. 1–10, 2023.

[12] P. Joshi, S. Ravi, Q. Liu, U. D. Bordoloi, S. Samii, S. K. Shukla, and H. Zeng, "Approaches for assigning offsets to signals for improving frame packing in CAN-FD," *IEEE Transactions on Computer-Aided Design of Integrated Circuits and Systems*, vol. 39, no. 5, pp. 1109–1122, 2019.

[13] H. Lim, G. Kim, S. Kim, and D. Kim, "Quantitative analysis of ringing in a controller area network with flexible data rate for reliable physical layer designs," *IEEE Transactions on Vehicular Technology*, vol. 68, no. 9, pp. 8906–8915, 2019.

[14] S. Kang, J. Seong, and M. Lee, "Controller area network with flexible data rate transmitter design with low electromagnetic emission," *IEEE Transactions on Vehicular Technology*, vol. 67, no. 8, pp. 7290–7298, 2018.

[15] R. Shirai, K. Wada, and T. Shimizu, "CAN signal processing for EMI reduction cooperating with switched-mode power supply," in *2020 IEEE Energy Conversion Congress and Exposition (ECCE)*. IEEE, 2020, pp. 3566–3571.

[16] L. Popa, A. Berdich, and B. Groza, "CarTwin—Development of a digital twin for a real-world in-vehicle CAN network," *Applied Sciences*, vol. 13, no. 1, p. 445, 2022.

[17] *CAN Specification Version 2.0.*, Robert BOSCH GmbH, 1991.

[18] I. O. for Standardization, "ISO11898-1. Road vehicles — Controller area network (CAN) —Part 1: Data link layer and physical signalling," International Organization for Standardization, Standard, 2nd edition, Dec 2015.

[19] ——, "ISO11898-2. Road vehicles — Controller area network (CAN) — Part 2: High-speed medium access unit," International Organization for Standardization, Standard, 2nd edition, Dec 2016.

[20] P.-S. Murvay and B. Groza, "TIDAL-CAN: Differential timing based intrusion detection and localization for controller area network," *IEEE Access*, vol. 8, pp. 68 895–68 912, 2020.

[21] B. Groza, P.-S. Murvay, L. Popa, and C. Jichici, "CAN-SQUARE-Decimeter level localization of electronic control units on CAN buses," in *Computer Security–ESORICS 2021: 26th European Symposium on Research in Computer Security, Darmstadt, Germany, October 4–8, 2021, Proceedings, Part I 26*. Springer, 2021, pp. 668–690.

[22] L. Popa, B. Groza, C. Jichici, and P.-S. Murvay, "ECUPrint—Physical fingerprinting electronic control units on CAN buses inside cars and SAE J1939 compliant vehicles," *IEEE Transactions on Information Forensics and Security*, vol. 17, pp. 1185–1200, 2022.